MODELING OF HIGH-POWER *Z* PINCHES

J. H. Hammer
J. S. De Groot
A. Toor
M. Tabak
P. Springer
K. Wong
G. Zimmerman

Introduction

Imploding *Z* pinches are powerful sources of x rays with application to weapons physics, weapons effects simulation, and inertial fusion. At drive powers of 20 TW and above, a pinch x-ray source heats materials to black body temperatures of order 100 eV or greater, enabling a variety of high-energy-density applications. Many of these applications, however, would benefit from a higher energy-density than achieved to date with *Z* pinches, placing a premium on understanding and controlling the pinch dynamics that limit the achievable energy density. For example, a factor of ~30 greater power density, as well as control of the x-ray pulse shape, may be required to employ a *Z* pinch as an ICF driver. Recent modeling work has shown the importance of RT instability in limiting the achievable power density of the pinch, and points to possible methods of reducing the effects of instabilities, which can lead to more useful high-power-density sources.

The *Z*-Pinch

Figure 1 is a sketch of the simplest pinch geometry, showing a pinch starting from an annular plasma shell or sheath. The sheath makes contact on each end with planar electrodes, and is created by electrical breakdown of an annular gas puff, wire array, cylindrical foil, or low-density foam. High voltage applied across the electrodes causes the breakdown and also causes a large electric current to flow in the direction of the cylindrical or *Z*-axis. The *Z*-current and resulting azimuthal magnetic field produce a radially directed force that implodes the pinch. The Saturn accelerator[1] at Sandia National Laboratories (SNL) drives *Z*-pinch loads at currents up to 10 MA, with a rise time of 50 ns and peak electrical power of 20 TW. The Z accelerator, also at SNL,[2,3] generates currents up to 20 MA with a rise time of 100 ns and peak electrical power of 40 TW.

X rays are produced when the imploding plasma reaches the axis. The implosion converts the electromagnetic energy of the driver into kinetic energy of the plasma, which becomes thermal energy at stagnation where the pinch collides with itself. The pinch is usually composed of a high-atomic-number material, such as W, that efficiently couples the plasma thermal energy to radiation. Saturn W wire-array pinches[4] have generated in excess of 0.5 MJ of x-ray energy at a peak power of 80 TW, while Z has produced 1.9 MJ of x rays at over 200 TW peak power.[5] The x rays can be used to drive an auxiliary experiment, including heating a hohlraum that encloses the *Z* pinch.

Although the energy and power of *Z*-pinch x-ray sources are high, the energy and power densities

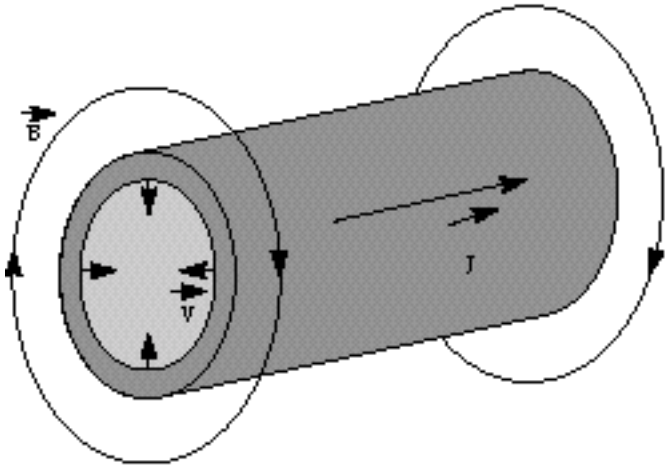

FIGURE 1. Imploding *Z* pinch configuration. B is the azimuthal magnetic field produced by the axial current J. V is the velocity resulting from the J × B force. (50-00-0797-1249pb01)

remain below those of laser-based sources, such as Lawrence Livermore National Laboratory's (LLNL's) Nova laser. The energy and power densities inside a hohlraum vary as the fourth power of the radiation temperature T_R, with critical minimum values of T_R required for inertial confinement fusion (ICF) or other high-energy-density experiments. For instance, successful ICF implosions[6] may require $T_R > 250$ eV. T_R is set by a balance between the input power and losses, which scale as the hohlraum area, so the highest T_R is achieved for the smallest-area hohlraum at a given power. T_R also depends on the hohlraum wall reflectivity, or albedo, which increases with T_R and time. In Saturn hohlraum experiments, the W wire-array pinch was surrounded with a gold radiation case (1 cm in radius and 2 cm long), producing peak T_R of 80 eV for a pinch-radiated power up to 80 TW with 4-ns pulse width.[7] At Nova, in comparison, values of T_R greater than 300 eV have been measured for 30 TW of laser power, nanosecond pulse lengths, and millimeter-size hohlraums.[8]

To increase the usefulness of *Z*-pinch x-ray sources, we are interested in increasing the energy density by decreasing the hohlraum size. The minimum *Z*-pinch hohlraum size is set by the initial pinch, radius, power feed gap, and the pinch length. The power feed gap is an annular slot on one end of the hohlraum between the sheath at radius $r = r_{sheath,}$ and the cylindrical hohlraum wall at $r = r_{sheath} + \Delta_{slot}$. Δ_{slot} is typically chosen to be 2 to 3 mm to avoid shorting out from plasma closure. If the sheath radius is not large enough to keep the initial inductance small, power flow is compromised by excessive voltage and current losses in the transmission line system. Saturn loads of 8-mm radius and below were fielded, while Z has required load radii of 10 mm or larger in initial experiments. Pinch lengths of at least 1 cm are thought to be needed to avoid excessive "end effects" where the imploding sheath interacts with the electrodes. Also, lengths of this order are considered necessary for good energy efficiency, which requires that the final pinch inductance (proportional to the length) be comparable with the driver inductance.

Higher currents and pinch energies can partially compensate for large loss areas in the effort to reach high T_R. At a given size, the energy scales approximately as the square of the current I, leading to T_R very roughly proportional to $I^{0.5}$ for similar pulsewidths and hohlraum dimensions. When Z can drive hohlraums similar in size to Saturn hohlraums, an improvement of roughly $(20/10)^{0.5}$ or T_R in the range 130–140 eV is expected and has recently been observed. Larger drivers in the 40–60-MA range are being planned, but it appears unlikely that $T_R > 250$ eV will be possible with this geometry, referred to as a *vacuum* hohlraum.

An alternative to the vacuum hohlraum is the *dynamic hohlraum*,[7] also known as the flying radiation case.[9] In this concept, the imploding pinch serves as the radiation case, trapping x rays produced when the imploding pinch strikes a "soda straw" or on-axis target. The x-ray energy is efficiently trapped if the imploding sheath is many optical depths in thickness. Because of the radial convergence, the dynamic hohlraum area can be dramatically reduced in comparison with the vacuum hohlraum, potentially leading to higher values of T_R.

The dynamic hohlraum places greater demands on our ability to predict and control plasma motion than the vacuum hohlraum. Control of the plasma is made difficult by magneto–Rayleigh–Taylor (RT) instability of the imploding sheath/hohlraum wall. The RT instability can lead to breakup of the hohlraum wall, permitting large losses of x-ray energy through holes and disruption of the symmetry due to the irregularity of the hohlraum wall. Fluid (nonmagnetic) RT instability can also be a problem when the hohlraum wall stagnates against low-density, low-opacity material interior to the dynamic hohlraum, causing mixing. Since the hohlraum wall is necessarily very opaque, the mixing could reduce the transport of x rays to a capsule or experiment of interest.

Aside from thermal x-ray sources, *Z*-pinches have also been used to generate K-shell x rays for weapons effects testing.[10] For this application, there is a need for higher-photon-energy (higher-atomic-number) K-shell radiators, which require both high implosion velocity for high temperatures and high stagnation densities to couple efficiently to radiation. As with the dynamic hohlraum, achieving these conditions places greater demands on control of the plasma dynamics, and RT modes in particular, than required for earlier, low-energy x-ray sources. The need for greater control motivates development of better theoretical and experimental understanding of imploding *Z* pinches.

Z-Pinch Modeling

A reliable predictive model for *Z* pinches does not yet exist, although there has been considerable recent progress. RT instability plays a central role in making the modeling difficult, as we can see from a simple argument. An imploding pinch does not have the benefit of ablative stabilization, as in ICF implosions, and resistive diffusion is ineffective at damping the most unstable modes.[11] The growth rate of the most unstable mode is given by the classical RT growth rate $\gamma = (kg)^{0.5}$, where $k = 2\pi/\lambda$, λ is the wavelength, and g the acceleration. For a uniformly accelerating sheath starting at radius $r_{0,}$ the implosion time is given by $t = (2r_0/g)^{0.5}$, leading to the number of e-foldings $N = \gamma t = (2kr_0)^{0.5}$. Pinch simulations with Saturn or Z current

waveforms and "matched" annular loads that couple efficiently to the driver give $N \approx (3kr_0)^{0.5}$. If we take a typical Z initial pinch radius of 15 mm and instability wavelength of 1 mm seen in x-ray framing images, we find $N = 17$. Such a large number of e-folding times indicates that the instability will be far into the nonlinear stage, making effective modeling a challenge.

2D, radiation magnetohydrodynamics (MHD) calculations confirm that strong growth of the RT instability plays a dominant role in the pinch dynamics. If the instability is ignored, as in 1D or under-resolved 2D calculations, the codes predict pinches that are orders of magnitude smaller in spatial extent and radiation output time than observed in experiments. Calculations including RT modes find x-ray pulse widths and magnitudes in reasonable agreement with experiments, as shown in Figure 2 for Saturn Al wire implosions. In all present calculations, however, there are at least two incomplete parts of the physics that limit our predictive capability: early time history and stagnation phase.

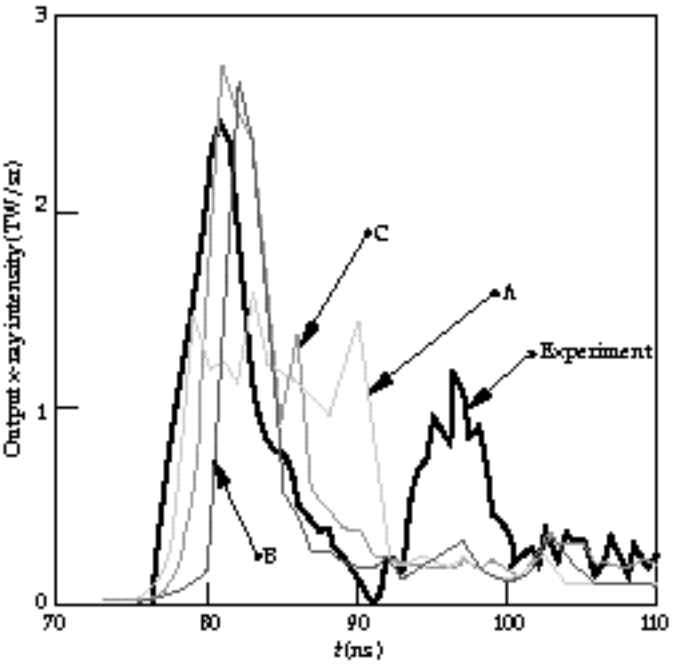

FIGURE 2. Saturn x-ray output power per unit solid angle measured by the bolometer in TW/sr compared with simulations: A, a single-mode density perturbation with amplitude 1% and wavelength 1 mm; B, a 1% random initial density perturbation with periodic boundary conditions and simulation length of 2 mm; C, a 5% random density perturbation with periodic boundary conditions and simulation length of 1 mm. (50-00-0797-1250pb01)

Early Time History

The first missing piece of physics concerns the early time history or initiation of the pinch. In the calculations, an initial density perturbation level is chosen arbitrarily, varying from 1% to 5% in the cases shown in Figure 2, which can cause a factor of 2 or greater variation in the x-ray pulse width. The pulse width is affected by the radial smearing of the mass from the breakup into RT bubble–spike structures. The RT growth sets the time scale for the stagnation on axis to $t_{stag} = t_{spike} - t_{bubble}$, where t_{spike} and t_{bubble} are the arrival times for the spike tip and bubble, respectively. Because the radiation is produced when kinetic energy is converted to thermal energy, the output radiation pulse also occurs in a time of order t_{stag}.

One approach to understanding the pinch initiation is to do finely zoned calculations modeling a small portion of the pinch. In these calculations, shown in Figure 3, we find that very small density-perturbation levels (~1 part in 1000) are sufficient to trigger large-amplitude RT instability. The modes that are initially excited have short wavelengths (~0.1 mm) and rapidly reach the nonlinear phase, consistent with the $1/\lambda^{0.5}$ scaling of the growth rate. The short wavelengths couple to longer (eventually ~1 mm) wavelength modes, creating a cascade similar to the behavior found in other classically RT unstable systems. After reaching the nonlinear stage, the calculations[12] show self-similar growth of a turbulent layer with width and dominant instability scale growing proportional to gt^2. This behavior is similar to the growth of mix layers in RT unstable fluid systems as described by Youngs.[13] Once the bubbles penetrate the entire sheath, the self-similar growth model breaks down, or at least changes in scaling coefficient. Also, once mode wavelengths approach the scale of the sheath thickness, resistive effects are more important and may cause deviation from the self-similar scaling. The early phase growth starting from short wavelengths may represent an "irreducible" seed for the long-wavelength modes that can ultimately disrupt the sheath. We are exploring ways to use fine-scale calculations to seed larger-scale calculations of the full implosion, as discussed further in the section on dynamic hohlraum modeling.

Wire-array pinches have the additional complication of the initial explosion and merging of the wires, which can create nonuniformities and seed RT modes. Recent experiments on Saturn and Z have found a strong dependence of the x-ray pulse width on the number of wires,[4,5,14] with much shorter pulses and higher power at large wire numbers. It is not known whether the improvement is due to reduced seeding of RT or other effects. The breakpoint in wire number where performance improves is close to the point where the expansion clouds from neighboring wires

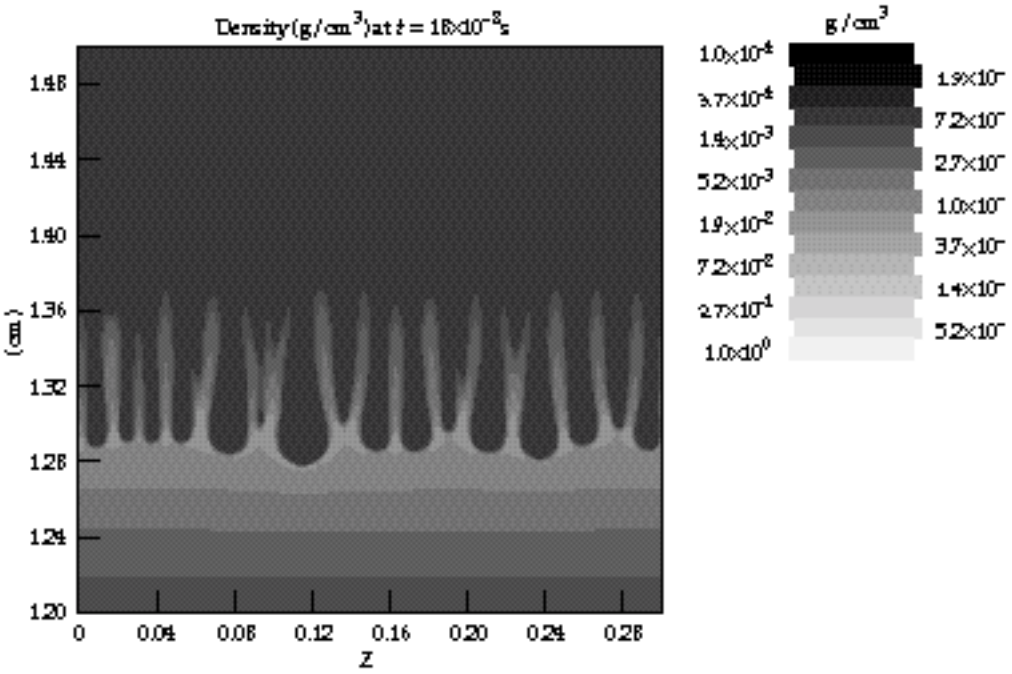

FIGURE 3. Density contours for a W Z pinch driven by Z. The problem is finely zoned with 10 × 10-μm zone size and an initial random density perturbation of 0.1%. The sheath was initialized as a nearly uniform block of 1-eV W vapor with a mean radius of 1.5 cm and width of 0.1 cm. (50-00-0707-1251pb01)

are expected to overlap.[14] The initial nonuniformity due to discrete wires is in the azimuthal direction, which is treated as uniform in the 2D RT calculations. Modes varying in the azimuthal direction behave differently because of the "field-line bending" effect that substantially lowers their growth rate. We hope to improve our understanding of wire-array initiation through calculations of the wire explosion and merging phases. Calculations are in progress using the TRAC2 radiation MHD code,[15] and experiments diagnosing wire initiation are planned at the University of Nevada.[16]

The large-wire-number Saturn and Z experiments may be approaching the "2D limit," where the pinch is fairly uniform in azimuth and dominated by rapidly growing azimuthally symmetric modes.

Stagnation Phase

A second missing piece of the physics applies to the stagnation phase. Our comparisons between calculation and experiment show that the radiating region is too dense and radially localized at stagnation, even for strongly RT-unstable pinches. Inclusion of 3D effects will likely be needed to resolve the differences. Because of the high radial convergence (~20), the effect of a relatively small azimuthal perturbation is strongly amplified. For instance, if a portion of the plasma develops angular momentum due to azimuthal nonuniformities, the energy associated with the angular motion increases as the square of the convergence ratio, making the plasma resistant to large radial compressions. If weak, as expected for large wire numbers and from the stabilization of field line bending, the 3D effects would have a small effect on the x-ray pulse width, yet would have a large effect on the pinch density and spatial scale at stagnation. The 3D effects are more important for self-stagnating than dynamic-hohlraum-type pinches because the latter strike an internal target and have lower convergence ratios.

Saturn Ne–Ar Gas-Puff Hohlraum Experiments

To benchmark and improve the 2D models, experiments were done on Saturn that permitted the first space- and time-resolved measurements of the density and T_e in the stagnating plasma.[17] Gas puff pinches composed of 90% Ne and 10% Ar were used for these experiments, and conditions at stagnation were measured with an absolutely calibrated, high-resolution space- and time-resolving x-ray spectrometer. The T_e was determined from the slope, as a function of photon energy, of the continuum radiation from recombining, fully stripped Ne ions. The ion density was found by measuring the Stark (or density-induced) broadening of spectral lines from He-like Ar ions.

For annular gas puffs (2 cm long, 1.25 cm initial r, 0.8 cm thick, and 600 μg total mass), the peak n_e at

stagnation was measured to be 8×10^{20} cm^{-3} with a corresponding peak mass density of 0.0028 g/cm^3, with a peak T_e of 1.2 keV. Figure 4 shows radial and axial profiles of the intensity of emission in two spectral energy bins (approximately proportional to the square of the density) and the radial and axial profile of T_e. The experimental data shown in Figure 4 are from a snapshot in time taken near peak x-ray emission. The axial variation is caused by "zippering" of the pinch where the sheath reaches the axis at different times. The middle of the pinch was observed to radiate first, followed by two localized emission spots that move outward toward the electrodes. The zippering is caused by initial axial variation of the gas puff, which is formed by releasing a supersonic gas jet into the vacuum.

We compared the data with 2D radiation MHD calculations with an initial large-scale density nonuniformity to simulate the zippering and with a 1% random zone-to-zone density perturbation to seed RT modes. We used two different atomic physics models. The first model assumes local thermodynamic equilibrium (LTE) where the populations of different atomic states are set equal to the values they would have in thermodynamic equilibrium at the local T_e. The second (non-LTE) model solves rate equations for the population of atomic states. Not surprisingly, for a comparatively low-density, hot plasma such as produced in the experiment, the non-LTE model differs markedly from the LTE model. The LTE model predicts a stagnation density of 0.33 g/cm^3, T_e of 300 eV, and a pinch diameter of 0.02 cm vs the observed pinch diameter of 0.2 cm. The 2D non-LTE model gives an improved stagnation density of 0.018 g/cm^3, a T_e of 700 eV, and a pinch diameter of 0.05 cm. The LTE model predicts stronger coupling to radiation than the non-LTE model, cooling the plasma so that it has less pressure to resist the radial collapse. The calculated intensity and T_e profiles from the 2D non-LTE run are shown in Figure 4 for comparison with the data. Figures 5 and 6 show a series of time snapshots of the plasma density and T_e during the implosion for the non-LTE run. The axial zippering and development of RT bubble-spike features are clearly visible in Figures 5 and 6.

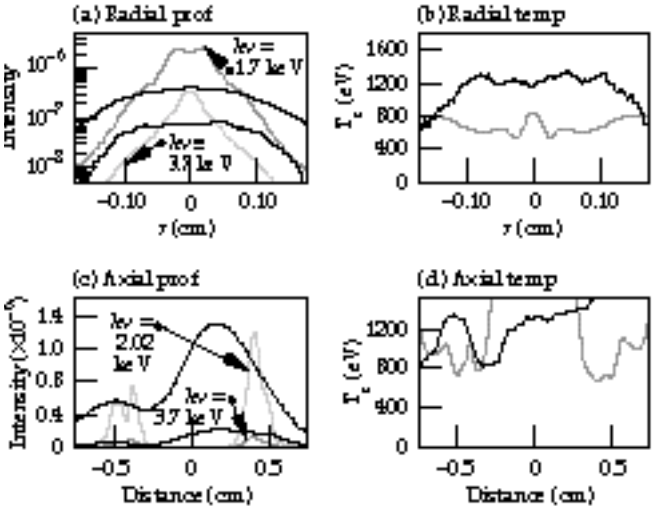

FIGURE 4. Radial and axial profiles of the intensity of emission in two different spectral energy bins near 1.7 keV and 3.7 keV. The intensity data are processed to give the radial and axial temperature profiles, also shown. Experimental data is shown in black, and the 2D non-LTE calculation is represented in gray. (50-00-0797-1252pb01)

We have also done a series of 1D non-LTE runs to determine whether the remaining differences are due to the atomic physics or other aspects of the modeling. We fix the pinch radius and density and add an ion heat source representing the shock heating at stagnation. At the radius and density of the 2D non-LTE simulation, the 1D runs also give a 700-eV T_e, while at the experimentally observed radius and density we calculate 1.2 keV in agreement with the experiment. These results suggest that the difference between the 2D model and experiment is not in the atomic physics, but in another part of the physics. The 2D hydrodynamic treatment is a likely source of the difference, perhaps requiring 3D as discussed above. Further support for this comes from broadband x-ray framing images of the implosion. The images show hoop-like structures during much of the implosion, as expected when viewing axially symmetric RT bubble–spike structures from an angle. At stagnation, however, the framing images show asymmetric features suggesting that a 3D treatment is needed. For both the 1D and 2D runs, the ion temperature (a few keV) is much lower than the 36-keV measured value from Doppler broadening. On the other hand, the emission-averaged turbulent flow energy from the 2D run is several tens of keV, suggesting that the Doppler-measured temperature actually measures plasma flow.

Z Dynamic Hohlraum Simulations

We have done 2D radiation MHD simulations of a dynamic hohlraum target designed to be driven by Z. In this design, we attempt to reduce the effects of RT modes by using a distributed initial density profile. In earlier work[11], we showed that "tailoring" the initial density profile could reduce the time-averaged sheath acceleration and number of *e*-foldings of the RT instability. As the sheath moves in radially, fresh material is swept up or "snow plowed," providing a back pres-

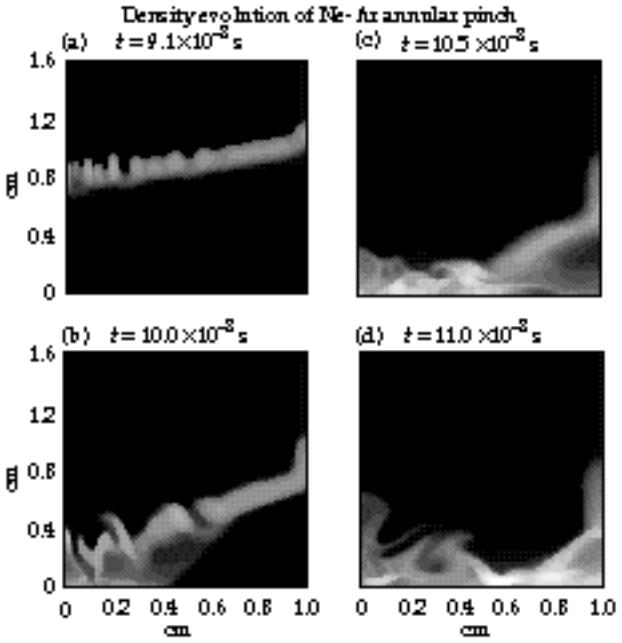

FIGURE 5. Density evolution of Ne–Ar annular pinch. Density contours are shown at times of 91, 100, 105, and 110 ns. (50-00-0797-1253pb01)

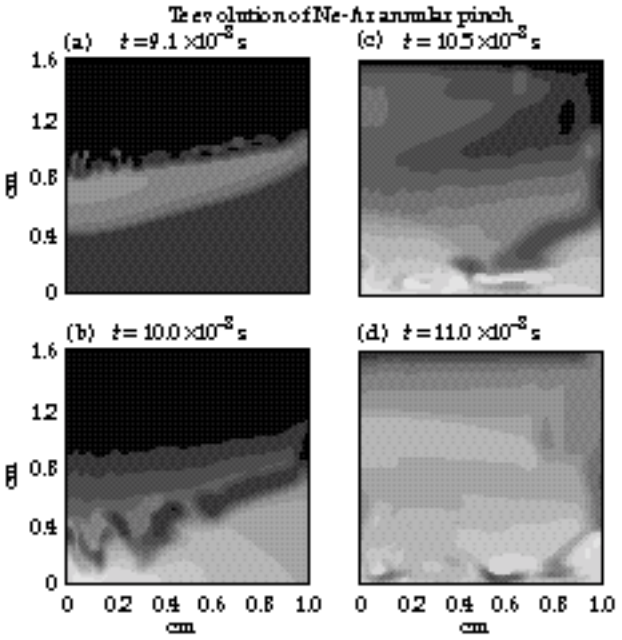

FIGURE 6. Electron temperature T_e evolution of Ne–Ar annular pinch. Temperature contours are shown at times of 91, 100, 105, and 110 ns. (50-00-0797-1254pb01)

sure that counters the **J** × **B** force.[18] A special profile can be found where the unstable outer surface of the sheath implodes at constant velocity, reducing the classical growth rate to zero, although residual Richtmeyer–Meshkov-type instability (instability of the snow-plow shock front) may be present. In practice, it is hard to create tailored initial density profiles due to the difficulty of machining and otherwise manipulating very-low-density materials. It becomes easier to manufacture these complex targets as the current, energy, and load mass increase with large drivers. *Z* is the first fast-pulse power device with enough energy to consider loads of this type.

The design we have modeled employs a 3-cm-diam, 2-cm-long W wire array of mass 7.54 mg as the high-atomic-number shell material. The wire array implodes on three concentric, annular shells of low-density (10-mg/cm^3) agar foam with a 25-μm layer of Be covering the interior of the central shell, shown in Figure 7. The annular shells, with foam between radii

of 1.1 and 1.15 cm (outer shell), 0.6 and 0.7 cm (middle shell), and 0.25 and 0.3 cm (inner shell), explode under the influence of the x rays emitted by the wire array and outer shells. In the process, they create a rough approximation to the zero-acceleration tailored density profile. The use of multiple shells to control RT instability in Z pinches has been studied previously.[19] Simulations in 1D show the stagnation of the Be at a minimum diameter of about 0.16 cm, with a peak radiation temperature of 240 eV and temperatures exceeding 200 eV for 7 ns. Figure 8 shows the radii of the different layers and the T_R on the pinch axis. The peak temperature occurs 50 ns after the current peaks at 17 MA. In the hot, stagnated Be, the average distance that x-ray photons can travel before being absorbed and reemitted, the Rosseland mean free path, is several times the pinch diameter, while the agar and W layers have an optical depth of about 20. With these conditions, it is sensible to describe the configuration as a dynamic hohlraum. The Be fills the hohlraum at a density of about 0.1 g/cm^3 and pressure of order 50 Mbar. This type of hohlraum is better suited to driving auxiliary experiments than ICF capsules inside the hohlraum that could be affected by the high plasma pressure. The drive temperature seen by an auxiliary experiment depends on the type of experiment. A highly reflective load on the end sees the full 240 eV, while a highly absorptive load removes significant energy from the hohlraum, dropping the effective drive temperature to 180 eV.

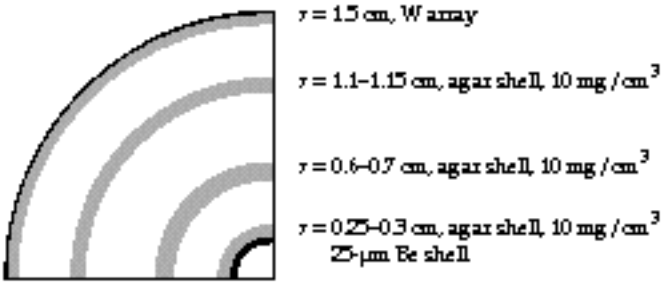

FIGURE 7. Dynamic hohlraum target. (50-00-0797-1263pb01)

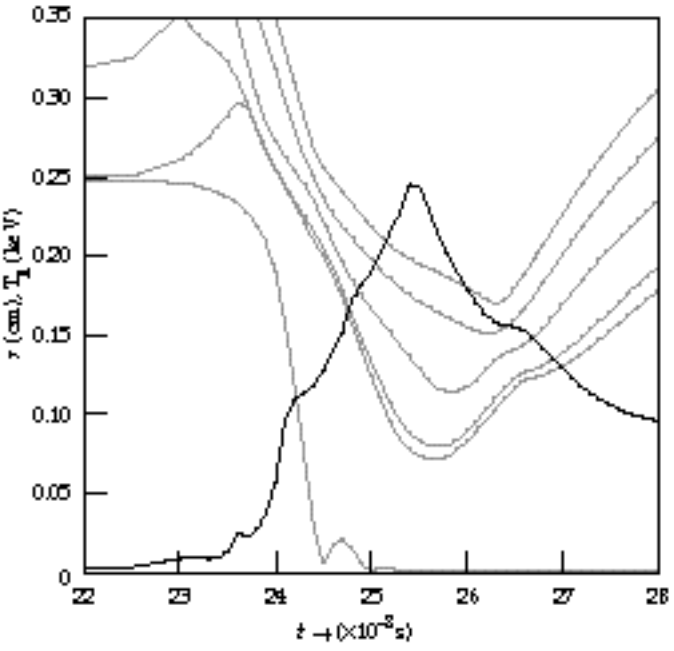

FIGURE 8. T_R (keV) on axis (solid line) and radius (cm) of shells (dashed lines) vs time(ns). (50-00-0797-1263pb01)

We have also done 2D calculations including the effects of RT modes for this target and similar designs. A calculation for a similar target with a 1% density perturbation and a 2-mm wavelength show significant instability growth in the W, but little perturbation of the inner layers. At stagnation against the inner annulus, the bubble–spike formation in the W is partly reversed. The peak temperature drops from 230 eV to ~220 eV, and the hohlraum interior remains optically thin at about the same diameter as the 1D simulation. Simulations of 2D with 5% initial random zone-to-zone density perturbation show larger amplitude growth in the W with less perturbation of the inner shells. The W is sufficiently disrupted that cracks in the radiation case form and allow large radial losses, causing the T_R on axis to drop to 180 eV. Perturbations in the 1% to 5% range have been found to give reasonable pulsewidths for Saturn and Z experiments,[11,20] although the perturbation level imposed in this way is zoning-dependent.

To reduce the uncertainty in choosing the perturbation level and come closer to a "first principles" RT calculation, we have done simulations with a very fine mesh. As discussed above, RT modes at short wavelengths can grow to nonlinear amplitudes very quickly from small initial perturbations, then seed more destructive long-wavelength modes through a nonlinear cascade. To provide a self-consistent instability seed, we have done a finely zoned (10-μm × 10-μm zones) calculation capable of resolving the short wavelengths that dominate the early phase. This method of initiating RT calculations with a 2D *r-z* code is only valid when there are enough wires in the initial array to merge into an azimuthally uniform sheath before significant RT growth begins. For this calculation, modeling 3 mm of the pinch length with periodic

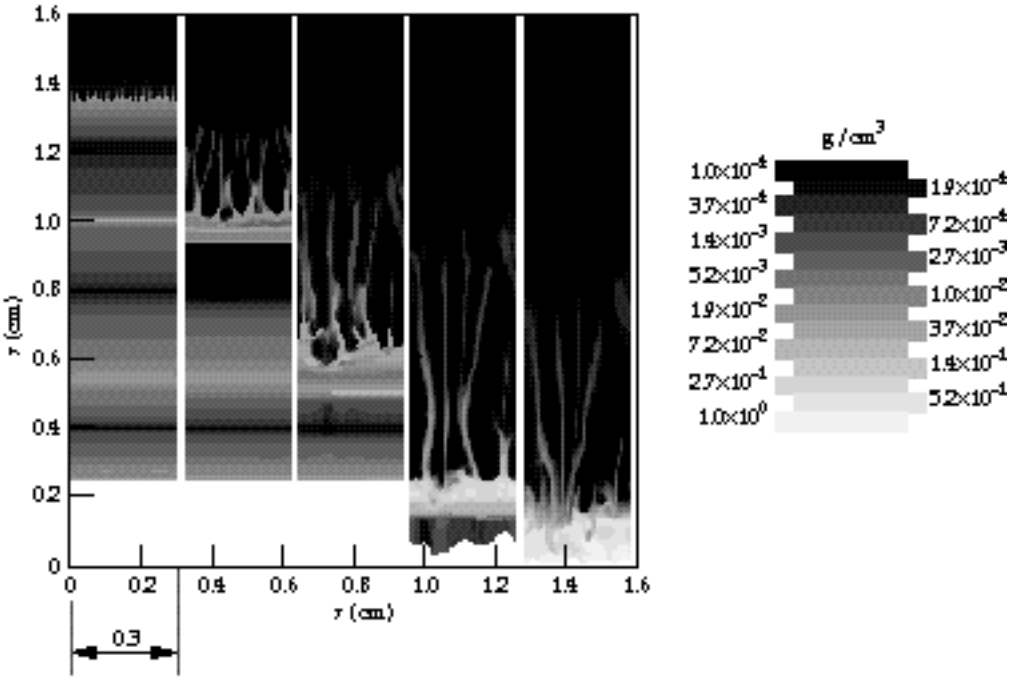

FIGURE 9. Density contours at 20-ns intervals in the 2D dynamic hohlraum simulation. (50-00-0797-1255pb01)

boundary conditions in the *z*-direction, random density perturbations of 0.1% were sufficient to stimulate large-amplitude RT growth. Once the dominant features were several hundred microns in scale, we linked to a coarser mesh (~30-μm zone size) to follow the complete implosion. A series of time snapshots of the plasma density for the multishell agar foam plus Be target are shown in Figure 9. This calculation showed reasonable integrity of the radiation case so that radiation leakage was not a major effect and the radiation temperature was ~220 eV in the hohlraum interior. A plume of optically thick, high-atomic-number material reached the axis at one location, however, which could inhibit energy flow to an adjacent load. If the high-atomic-number plume occurs more than a few mm from the output end, the effect on energy flow should be small. The RT calculations do not include the effect of an x-ray-absorbing load, which would cause an additional drop in the T_R.

All of the calculations show significant breakup of the W sheath before it encounters the outermost stabilizing agar shell. This prompts us to consider an initial state that more closely approximates the zero-acceleration density profile at large radius. At present, it is not practical to extend the profile to larger radius with low-density foams because of our limited ability to machine and handle these extremely fragile materials. An alternative may be to use concentric, nested wire arrays, with the separation between wires in each shell smaller than the distance the wires expand due to heating by x rays. With this technique, an arbitrary initial density profile of virtually any material may be possible. The first experiments with simpler loads will indicate if these more complex targets are necessary to control RT instability.

Conclusion

Imploding pinches have produced very powerful and energetic x-ray sources, yet our understanding of the basic dynamics of these devices is still at an early stage. The initiation of the pinch, in particular, is critical to the subsequent dynamics but remains poorly understood. Recent modeling work has shown the importance of RT instability in limiting the achievable power density of the pinch and points to possible methods of reducing the effects of instabilities through control of the initial density distribution. Developing efficient, reproducible, high-power-density sources (>250 eV) is likely to require control of instabilities. We anticipate that further research will enable us to develop a better understanding of pinch dynamics, which may lead to higher energy densities of greater use to the Department of Energy's Stockpile Stewardship and Management Program.

Notes and References

1. D. D. Bloomquist, R. M. Stinnett, D. H. McDaniel, J. R. Lee, et al., *Proc. 6th International Electrical and Electronic Engineering Pulsed Power Conference*, Arlington, VA, Eds., P. J. Turchi and B. H. Bernstein (IEEE, New York, 1987), p. 310.
2. R. B. Spielman, et. al., "Paper O–4–3," in *Proceedings of the 10th International Conference on High Power Particle Beams*, Prague, Czech Republic, June 10–14, 1996, Eds., K. Jungwirth and J. Ullschmied, pp. 150–153. (Copies of the conference proceedings can be ordered from *BEAMs96*, Institute of Plasma Physics, Czech Academy of Sciences, Za Slovankou 3, 182 00 Prague, Czech Republic.)
3. R. B. Spielman, G. A. Chandler, C. Deeney, F. Long, T. H. Martin, M. K. Matzen, et al., *Bull. Am. Phys. Soc.* **41**, 1422 (1996).
4. C. Deeney, T. J. Nash, R. B. Spielman, J. F. Seamen, et al., "Power Enhancement by Increasing Initial Array Radius and Wire Number of Tungsten Z Pinches," submitted to *Phys. Rev. E.*
5. R. B. Spielman, Sandia National Laboratory, Albuquerque, NM, private communication (1997).
6. J. Lindl, *Phys. Plasmas* **2**, 3933 (1995).
7. M. K. Matzen, *Phys. Plasmas* **4**, 1519 (1997).
8. R. Kauffman, L. Suter, C. B. Darrow, J. D. Kilkenny, et al., *Phys. Rev. Lett.* **73**, 2320 (1994).
9. J. Brownell, Los Alamos National Laboratory, Los Alamos NM, private communication (1995).
10. C. Deeney, T. Nash, R. R. Prasad, L. Warren, et al., *Phys. Rev. A* **44**, 6762 (1991).
11. J. H. Hammer, J. L. Eddleman, P. T. Springer, M. Tabak, et al., *Phys. Plasmas* **3**, 2063 (1996).
12. J. H. Hammer, J. L. Eddleman, M. Tabak, A. Toor and G. B. Zimmerman, "Sheath Broadening in Imploding Z-pinches due to Large-bandwidth Rayleigh-Taylor Instability," in *Proceedings of the 10th International Conference on High Power Particle Beams*, Prague, Czech Republic, June 10–14, 1996, Eds. K. Jungwirth and J. Ullschmied. (Copies of the conference proceedings can be ordered from *BEAMs96*, Institute of Plasma Physics, Czech Academy of Sciences, Za Slovankou 3, 182 00 Prague, Czech Republic.)
13. D. L. Youngs, *Physica* **12D**, 32 (1984).
14. T. W. L. Sanford, G. O. Allshouse, B. M. Marder, T. J. Nash, et. al., *Phys. Rev. Lett* **77**, 5063 (1996).
15. J. L. Eddleman, J. H. Hammer, C. W. Hartman, A. W. Molvik, and H.S. McLean, *Bull. Am. Phys. Soc.* **34**, 2051 (1989).
16. B. S. Bauer, Department of Physics, University of Nevada, Reno, private communication (1997).
17. K. L. Wong, P. T. Springer, J. H. Hammer, C. A. Iglesias, et. al., "Spectroscopic Characterization of an Argon-Neon Z-Pinch Plasma at Stagnation," in preparation, July 1997.
18. A. L. Velikovich, F. L. Cochran, and J. Davis, *Phys. Rev. Lett.* **77**, 853 (1996).
19. R. B. Baksht, S. P. Bugaev, I. M. Datsko, A. V. Luchinskii, et al., "Dense Z-Pinches, Tjore International Conference," Eds. M. Haines and A. Knight (AIP Conference Proceedings, vol. 299, p. 365, AIP, New York), 1994.
20. D. L. Peterson, R. L. Bowers, J. H. Brownell, A. E. Greene, et al., *Phys. Plasmas* **3**, 368 (1996).